

Enhanced Catalytic Performance of Fe-containing HZSM-5 for Ethane Non-Oxidative Dehydrogenation via Hydrothermal Post-Treatment

Lizhi Wu,^{*,[a]} Zhiyuan Fu,^[a] Zhuangzhuang Ren,^[a] Jinhe Wei,^[a] Xinhua Gao,^[b] Li Tan,^[a] and Yu Tang^[a]

A facile strategy is applied to construct Fe supported ZSM-5 (Fe/HZ5-HTS) via hydrothermal post-treatment and applied to ethane non-oxidative dehydrogenation. Compared with Fe/HZ5-IWI prepared by incipient wetness impregnation, Fe/HZ5-HTS exhibits superior catalytic activity and long catalyst stability with 6000 minutes time-on-stream. An obvious volcanic curve is observed between the ethylene generation rate and Fe content, and 1.0Fe/HZ5-HTS exhibits the highest ethylene generation rate with $0.166 \text{ mmol C}_2\text{H}_4 \text{ s}^{-1} \text{ g}_{\text{Fe}}^{-1}$ over different Fe loading, which is twice as much as that of 1.0Fe/HZ5-IWI. According to

various characterizations, isolated Fe^{3+} species and carburized Fe species are active sites, and the better catalytic performance over 1.0Fe/HZ5-HTS is ascribed to more disperse Fe species and exposing more Fe species in the surface. Besides, the lower ethylene desorption temperature and higher ethane desorption temperature over Fe/HZ5-HTS could suppress the overreaction of the ethylene to generate coke and increase ethane residence reaction time, resulting in less coke deposition and facilitating the catalytic performance.

Introduction

Ethylene is one of the most important chemical intermediates in the petrochemical industry.^[1] Currently, the industrial-scale production of ethylene is mainly based on steam cracking of hydrocarbon feedstocks, including gaseous alkanes and liquid petroleum products, which is highly energy intensive and requiring high temperature.^[2] Recently, with the development of shale gas exploration technology, the production of ethylene through ethane cracking route has attracted extensive attention with great advantages, such as lower production cost, high ethylene yield and less equipment investment compared with conventional naphtha pyrolysis, as an environmentally benign chemical process.^[1a,3]

Ethane dehydrogenation includes oxidative dehydrogenation (ODH) and non-oxidative dehydrogenation. Oxidative dehydrogenation of ethane with different oxidizing agents (such as O_2 , CO_2 and N_2O) has attracted great attention, coupling the endothermic dehydration of ethane with the strongly exothermic oxidation of hydrogen, which has higher thermodynamic conversion and avoids the need for excessive

internal heat input.^[3e,4] However, oxidative dehydrogenation suffers great challenge on the low selectivity of ethylene due to over-oxidation of ethane to carbon dioxide, as well as the heat recovery and process safety control owing to the highly exothermic nature of the oxidative dehydrogenation process.^[4a,f,5] On the other hand, non-oxidative dehydrogenation of ethane (EDH) could avoid most of the disadvantages along with high selectivity of ethylene compared with ODH. The drawbacks of non-oxidative dehydrogenation are relatively high energy demand, low single-pass conversion limited by the thermodynamic equilibrium, and rapid deactivation of catalyst from coking.^[5-6]

Currently, non-oxidative dehydrogenation catalyst of light alkanes, such as ethane and propane, mainly contains Pt–M (M=Sn, Zn, Ga, In)^[6d,i,7] and CrO_x ^[6a-c,g-j,m] supported catalyst, as the most extensively studied systems owing to its high activity. Nevertheless, owing to environmentally unfriendly CrO_x -based catalyst, and high-cost as well as easily agglomeration of Pt–M catalyst, it is urgent to develop highly active, selective as well as coke-resistant catalysts.

HZSM-5, a typical MFI-type zeolite, has been widely applied in the chemical industry, such as alkylation, isomerization and aromatization catalyst of light alkanes.^[8] On the other hand, owing to the tri-dimensional micropore structure, large specific surface area, appropriate acidity and thermally stable, HZSM-5 is considered to be a good catalyst support. It is extensively reported that Fe supported HZSM-5 displayed high reactivity on oxidative dehydrogenation of propane to propene with N_2O as oxides, which is ascribed to the radical-type character of the Fe(III)-O^- species when Fe species contacting N_2O .^[9] Recently, Fe/HZ5 is found to be active in non-oxidative dehydrogenation of ethane, carburized Fe species and metallic Fe species are

[a] Dr. L. Wu, Z. Fu, Z. Ren, J. Wei, Prof. L. Tan, Prof. Y. Tang
Institute of Molecular Catalysis and In-situ/operando Studies
College of Chemistry
Fuzhou University
350108 Fuzhou (P. R. China)
E-mail: wulz@fzu.edu.cn

[b] Prof. X. Gao
State Key Laboratory of High-Efficiency Utilization of
Coal and Green Chemical Engineering
College of Chemistry and Chemical Engineering
Ningxia University
750021 Yinchuan (P. R. China)

Supporting information for this article is available on the WWW under
<https://doi.org/10.1002/cctc.202100752>

No.	Samples	Fe loading ^[a] [wt%]	Si/Al ratio ^[a]	$S_{\text{BET}}^{[b]}$ [m ² g ⁻¹]	$V_{\text{micro}}^{[b]}$ [cm ³ g ⁻¹]	$V_{\text{meso}}^{[b]}$ [cm ³ g ⁻¹]	Total acidity ^[c] [mmolNH ₃ g ⁻¹]
1	HZSM-5	/	29.0	331	0.144	0.055	0.517
2	0.5Fe/HZ5-IWI	0.43	28.9	322	0.135	0.077	0.449
3	1.0Fe/HZ5-IWI	0.89	27.8	324	0.138	0.064	0.426
4	2.0Fe/HZ5-IWI	1.83	28.2	314	0.139	0.057	0.432
5	0.5Fe/HZ5-HTS	0.51	28.5	364	0.088	0.188	0.514
6	1.0Fe/HZ5-HTS	0.83	28.8	369	0.078	0.217	0.443
7	2.0Fe/HZ5-HTS	1.72	28.5	376	0.059	0.179	0.438
8	1.0Fe/HZ5-meso-IWI ^[d]	0.90	28.1	367	0.097	0.176	0.418
9	1.0Fe/Silicalite-1-IWI	0.93	/	358	0.113	0.141	/

[a] Detected by ICP-OES analysis, [b] Calculated by BET method. S_{BET} , V_{micro} and V_{meso} stand for specific surface area, microporous volume and mesoporous volume, respectively, [c] Determined from NH₃-TPD, [d] Catalyst was prepared via incipient wetness impregnation of Fe precursor to mesoporous ZSM-5.

supposed to be the active sites for EDH reaction, which exhibits both high activity and excellent stability.^[10]

In this present work, we propose a facile strategy to construct Fe supported ZSM-5 (Fe/HZ5-HTS) via hydrothermal post-treatment of the conventional HZSM-5 with the introduction of Fe precursor. Compared with the conventional incipient wetness impregnation method (Fe/HZ5-IWI), it is found that the new Fe/HZ5-HTS demonstrates to be highly active and long catalyst stability with less coke deposition on non-oxidative dehydrogenation of ethane. According to the systematic characterizations including TEM, UV/Vis, NH₃-TPD, H₂-TPR, XPS and TG results, isolated Fe³⁺ species and carburized Fe species are supposed to be the active sites over EDH, and the high-performance of Fe/HZ5-HTS could be ascribed to the more dispersive Fe species over HZSM-5 and exposing more Fe active sites including carburized Fe species and metallic Fe species in the surface. And it is found that the relatively lower ethylene desorption temperature and higher ethane desorption temperature over Fe/HZ5-HTS are observed, which could suppress the overreaction of the ethylene to generate coke and increase corresponding ethane residence reaction time, respectively, and facilitate the catalytic performance correspondingly.

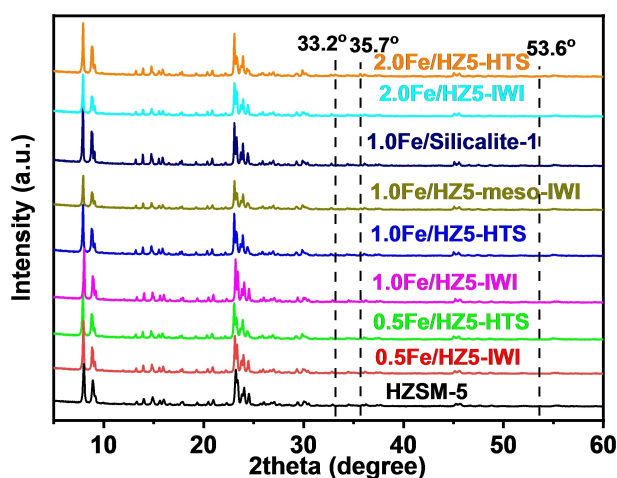


Figure 1. Representative XRD patterns of ZSM-5, Fe/HZ5-IWI and Fe/HZ5-HTS with different Fe content.

Results and Discussion

The XRD patterns (Figure 1) of all the prepared samples present the representative peaks at 7–9° and 23–24°, indicating all the samples of framework structure of MFI host are well preserved after introducing Fe species. Besides, no diffraction peaks of Fe₂O₃ (33.2°, 35.7°, and 53.6°) or other metallic Fe species^[10a,11] are observed over prepared Fe/HZ5 samples, indicating that the Fe species are highly dispersed over HZSM-5 support.

The detailed textural properties of catalysts based on the N₂ adsorption at 77 K, ICP, NH₃-TPD have been concluded in Table 1. The Fe content of each Fe/HZ5 sample is close to nominal value. As for Fe/HZ5-IWI catalysts, it is found that the BET surface area, microporous and mesoporous volume keep almost unchanged compared with parent HZSM-5 sample regardless of the different Fe loading, and the corresponding N₂ physisorption shows an adsorption branch of type I isotherm (Figure 2a–d), typical for microporous materials. Nevertheless, when Fe is introduced into HZSM-5 via alkali hydrothermal post-treatment, the BET surface area and mesoporous volume of Fe/HZ5-HTS samples with different Fe content increase 33–45 m²g⁻¹ and 0.124–0.162 cm³g⁻¹, respectively, and the corre-

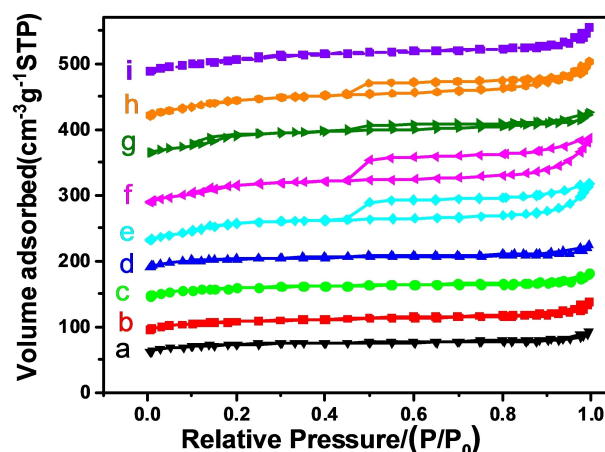


Figure 2. N₂ physisorption isotherms for HZSM-5, Fe/HZ5-IWI and Fe/HZ5-HTS. (a) HZSM-5; (b) 0.5Fe/HZ5-IWI; (c) 1.0Fe/HZ5-IWI; (d) 2.0Fe/HZ5-IWI; (e) 0.5Fe/HZ5-HTS; (f) 1.0Fe/HZ5-HTS; (g) 2.0Fe/HZ5-HTS; (h) 1.0Fe/HZ5-meso-IWI; (i) 1.0Fe/Silicalite-1.

spending N₂ physisorption shows an adsorption branch of type IV isotherm (Figure 2e–g), indicating the existence of mesopores, which is ascribed to the hydrothermal alkali treatment environment resulting in the Si dissolution to generate mesoporous. To further eliminate that the existence of mesopore may possibly influence the EDH performance, mesopore included sample 1.0Fe/HZ5-meso-IWI (Table 1 No. 8, Figure 2 h) is prepared according to incipient wetness impregnation of Fe precursor to mesoporous HZSM-5 as described in experimental Section.

The catalyst acidity is further characterized by NH₃-TPD, as shown in Figure 3. The NH₃-TPD profiles for HZSM-5, Fe/HZ5 samples all show two major desorption peaks at around 210 °C and 420 °C, which could be assigned to that NH₃ strongly adsorbed on the weak acid sites and strong acid sites of HZSM-5.^[12] It could be found that with the incremental Fe content over Fe/HZ5-IWI and Fe/HZ5-HTS, the peak intensity at 420 °C decreases gradually, which indicates the strong acid sites of HZSM-5 is preferred to be neutralized. Correspondingly, the total amount of acid sites after introducing Fe species decreases based on the further quantitative analysis of desorbed NH₃ (Figure 3 and Table 1). The decreased acidity over Fe/HZ5 samples could be ascribed to that the introduction of Fe species exchanges the Brønsted acid protons of Si–O(H)–Al. On the

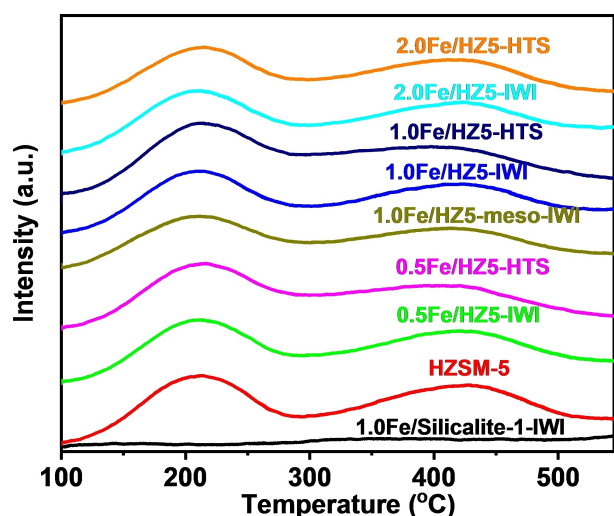


Figure 3. NH₃-TPD profiles of HZSM-5, Fe/HZ5 and Fe/Silicalite-1.

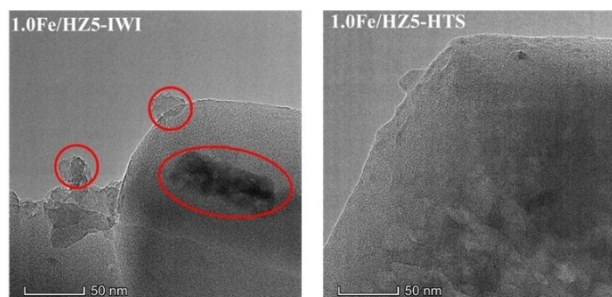


Figure 4. TEM images of Fe/HZ5-IWI and Fe/HZ5-HTS.

other hand, it is found the acid sites in 1.0Fe/Silicalite-1-IWI is very weak since no existence of Al sites.

Figure 4 and Figure 5 show the TEM and STEM-EDS elemental mapping of 1.0Fe/HZ5-IWI and 1.0Fe/HZ5-HTS, which could be used to evaluate the dispersion of the Fe species. It is obvious that some small, aggregated Fe oxides nanoparticles could be observed over 1.0Fe/HZ5-IWI, while it is hardly to see the Fe oxides nanoparticles over 1.0Fe/HZ5-HTS from the TEM images in Figure 4, which could be concluded that Fe species over 1.0Fe/HZ5-HTS is highly dispersed compared with that of 1.0Fe/HZ5-IWI. In addition, EDS mapping is further used to illustrate the corresponding element distribution (Figure 5), it is found the element of Si, O, Al distribute homogeneously over 1.0Fe/HZ5-IWI and 1.0Fe/HZ5-HTS samples. Nevertheless, Fe element distributes non-homogeneously obviously over 1.0Fe/HZ5-IWI with aggregated Fe oxides clusters on both edges, while the Fe element distributes homogeneously over 1.0Fe/HZ5-HTS. The TEM and further EDS mapping results demonstrate that the Fe species are highly dispersed over support HZSM-5 via hydrothermal alkali post-treatment compared with conventional incipient wetness impregnation.

To further distinguish different Fe species, H₂-TPR is conducted to understand the corresponding Fe species structure over different catalysts, as shown in Figure 6. Three major peaks at 350, 450 and 550 °C appear over 2.0Fe/HZ5-IWI and 2.0Fe/HZ5-HTS samples (Figure 6A), which could be ascribed to the reduction peaks of Fe₂O₃, Fe₃O₄, and FeO species, respectively.^[13] This suggests that the Fe species are similar when Fe loading is 2.0 wt% regardless of Fe introduction manner, and exists mainly in the manner of iron oxides. Nevertheless, when Fe content is further decreased to 1.0 wt% or less, it could be found that Fe introduction manner affects Fe states greatly. As for 1.0Fe/HZ5-IWI and 1.0Fe/Silicalite-1-IWI via incipient wetness impregnation (Figure 6B), the obvious peaks at 350, 450 and 550 °C representing Fe₂O₃, Fe₃O₄ and FeO species are still observed, indicating that mostly Fe species still exist in the manner of iron oxides. On the other hand, it is found that only slight peaks at 350 and 550 °C corresponding to Fe₂O₃ and FeO species appear over 1.0Fe/HZ5-HTS, and the corresponding peak intensity is obviously lower than that of 1.0Fe/HZ5-IWI. When the Fe loading is further decreased to 0.5 wt%, the corresponding Fe reduction peaks intensity over 0.5Fe/HZ5-HTS is also lower than that of 0.5Fe/HZ5-IWI (Figure 6C). Above H₂-TPR experimental results demonstrate that the Fe species over 0.5Fe/HZ5-HTS and 1.0Fe/HZ5-HTS is difficult to be reduced compared with that of Fe/HZ5-IWI, which could be ascribed to that a more highly dispersed Fe species in HZSM-5 and a stronger interaction between Fe sites and HZSM-5 support, which is in accordance with previous TEM and EDS mapping results.

UV/Vis spectra is further used to investigate the nature of Fe species in Fe-zeolite samples, the corresponding UV/Vis spectra of the Fe/HZ5-IWI and Fe/HZ5-HTS are compared in Figure 7. According to literature report, bands below 300 nm are assigned to isolated Fe³⁺ sites with two ligand-to-metal charge-transfer transitions, t₁→t₂ and t₁→e, whereby their specific position depends on the number of ligands.^[14] From the UV/Vis

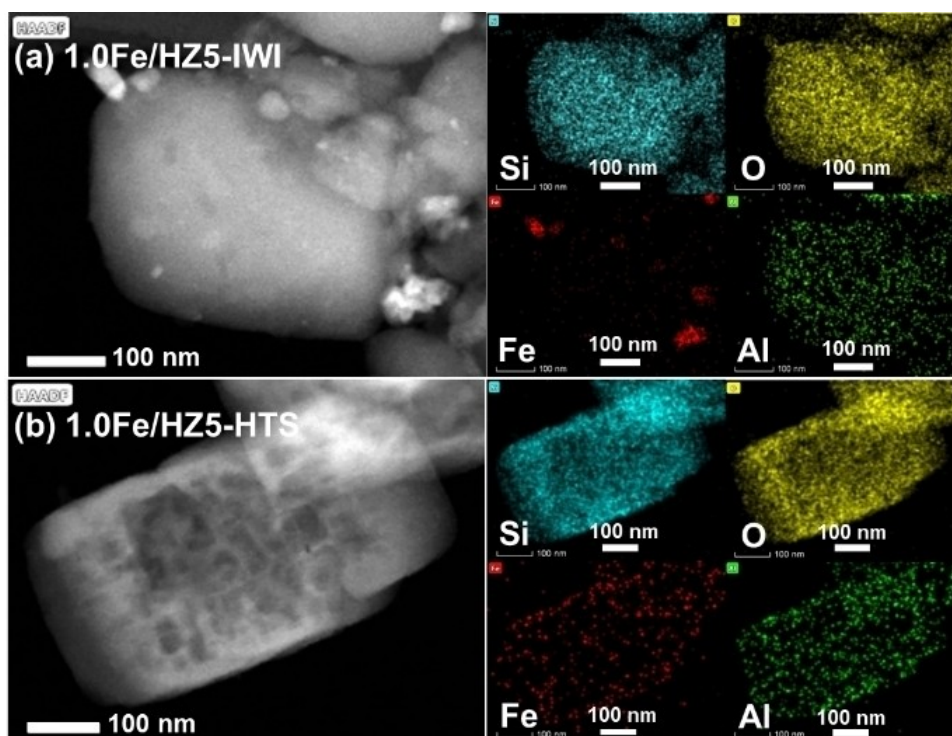


Figure 5. HAADF-STEM images and the corresponding elemental mapping of 1.0Fe/HZ5-IWI (a) and 1.0Fe/HZ5-HTS (b).

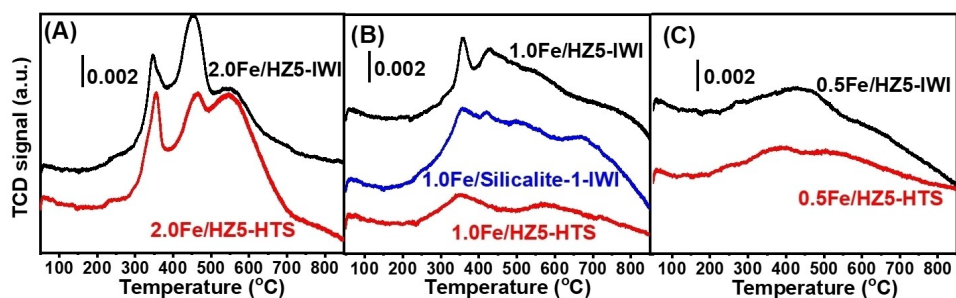


Figure 6. H₂-TPR profiles of Fe/HZ5-IWI and Fe/HZ5-HTS.

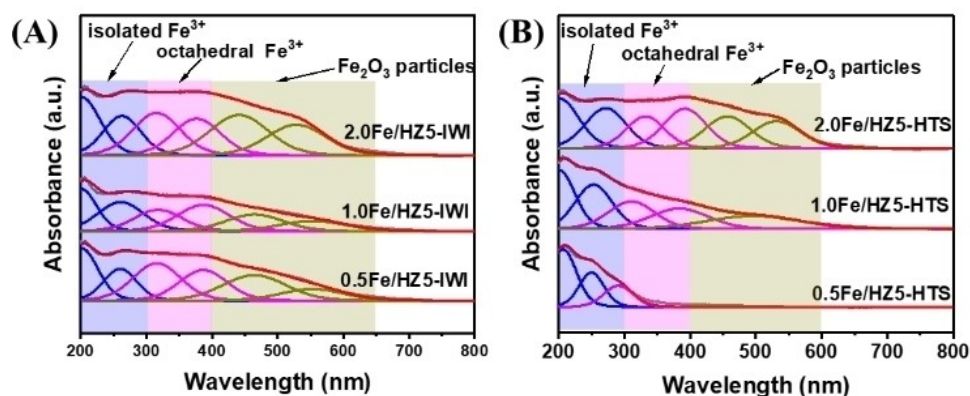


Figure 7. UV/Vis spectra of Fe/HZ5-IWI (A) and Fe/HZ5-HTS (B) with different Fe content.

spectra of the Fe/HZ5-IWI and Fe/HZ5-HTS in Figure 7, two bands appear at 210 nm and 251 nm over Fe/HZ5-HTS samples (Figure 7B), corresponding to isolated tetrahedral and high coordination Fe^{3+} sites. On the other hand, corresponding isolated tetrahedral Fe^{3+} sites absorption band over Fe/HZ5-IWI appears at 210 nm and high coordination Fe^{3+} sites absorption band is red-shifted to 271 nm compared with Fe/HZ5-HTS, indicating the higher coordination of Fe^{3+} sites over Fe/HZ5-IWI.^[14a] In addition, bands at 300–400 nm and >400 nm are observed over both Fe/HZ5-IWI and Fe/HZ5-HTS catalysts, which are assigned to octahedral Fe^{3+} in small oligomeric Fe_xO_y clusters and large Fe_2O_3 particles, respectively.^[14] To further estimate the Fe species distribution with Fe content and Fe introduction manner, the UV/Vis spectrum of Fe/HZ5-IWI and Fe/HZ5-HTS catalysts with different Fe content is deconvoluted with $r^2 > 0.999$, and the results are summarized in Table 2. Correspondingly, the percentage of isolated Fe^{3+} sites, oligomeric Fe_xO_y clusters and Fe_2O_3 particles could be confirmed semi-quantitative over Fe/HZ5-IWI and Fe/HZ5-HTS with the analysis of deconvoluted data (Table S1). And it is surprised to find that Fe introduction manner would result in different Fe species distribution. As for Fe/HZ5-IWI with different Fe content, it could be found that the content of isolated Fe^{3+} sites is about 25–32%, while corresponding oligomeric Fe_xO_y clusters and Fe_2O_3 particles are 36–43% and 28–39%, respectively, which indicating that major Fe species over Fe/HZ5-IWI exist in the manner of oligomeric Fe_xO_y clusters and large Fe_2O_3 particles. On the other hand, when Fe is introduced via hydrothermal

post-treatment over Fe/HZ5-HTS catalysts, it could be found that the content of isolated Fe^{3+} sites is about 41–74%, which is obviously higher than that of Fe/HZ5-IWI. While corresponding oligomeric Fe_xO_y clusters and Fe_2O_3 particles are 26–40% and 0–29%, lower than that of Fe/HZ5-IWI. And it is worth noting that when Fe loading is rather high (2.0%), corresponding large Fe_2O_3 particles are highest, which indicated that high Fe content loading is not beneficial for Fe species homogeneous distribution.

To further identify the surface state of iron ions on incipient wetness impregnation and hydrothermal alkali post-treatment catalysts, the samples are characterized by XPS spectra. The corresponding Fe 2p XPS spectra of prepared fresh catalysts are shown in Figure 8A, which contains two components at BE of ~ 711 eV (Fe $2p_{3/2}$) and ~ 724 eV (Fe $2p_{1/2}$), respectively. It is noted that the corresponding peaks intensity of 1.0Fe/HZ5-HTS is obviously higher than that of 1.0Fe/HZ5-IWI, the further surface atomic concentration analysis show that the surface Fe atomic concentration over 1.0Fe/HZ5-HTS is 1.75 at.%, which is much higher than that of 1.0Fe/HZ5-IWI (0.52 at.%). The higher Fe content in the surface over 1.0Fe/HZ5-HTS could facilitate the catalytic reaction correspondingly. In addition, to further confirm the corresponding Fe state, the further curve fitting result of Fe2p spectrum over 1.0Fe/HZ5-HTS is shown in Figure 8A and (Table S2) (the signal intensity of 1.0Fe/HZ5-IWI is too low and could not fit properly), it could be found that peaks appear with main peaks at 711.0 eV, 712.9 eV representing octahedral and tetrahedral Fe^{3+} species, and along with shoulder peaks at 709.6 eV corresponding to octahedral Fe^{2+} species,^[10a] which indicates Fe species mainly exists in the manner of isolated Fe^{3+} over Fe/HZ5-HTS, in accordance with previous UV/Vis characterization result.

In addition, the further situ Raman and Drifts-CO characterization results are shown in Figure S1 and Figure S2. As for situ Raman results, besides the bands at 380 and 800 cm^{-1} corresponding to characteristic of MFI structure of ZSM-5,^[15] bands at 600 and 433 cm^{-1} ascribed to bulky Fe_2O_3 aggregates also appear over both Fe/HZ5-IWI and Fe/HZ5-HTS. And it is noted that band at 1063 cm^{-1} corresponding to asymmetric -Fe-O-Si- stretching vibrational appears on both catalysts,^[15] and the corresponding bands intensity over Fe/HZ5-HTS at

No.	Sample	$I_1^{[a]}$ [%]	$I_2^{[b]}$ [%]	$I_3^{[c]}$ [%]
1	0.5Fe/HZ5-IWI	25	43	32
2	1.0Fe/HZ5-IWI	32	40	28
3	2.0Fe/HZ5-IWI	25	36	39
4	0.5Fe-HZ5-HTS	74	26	0
5	1.0Fe-HZ5-HTS	41	40	19
6	2.0Fe-HZ5-HTS	41	30	29

[a] Isolated Fe^{3+} in tetrahedral and higher coordination, [b] Small oligomeric Fe_xO_y clusters, [c] Large Fe_2O_3 particles.

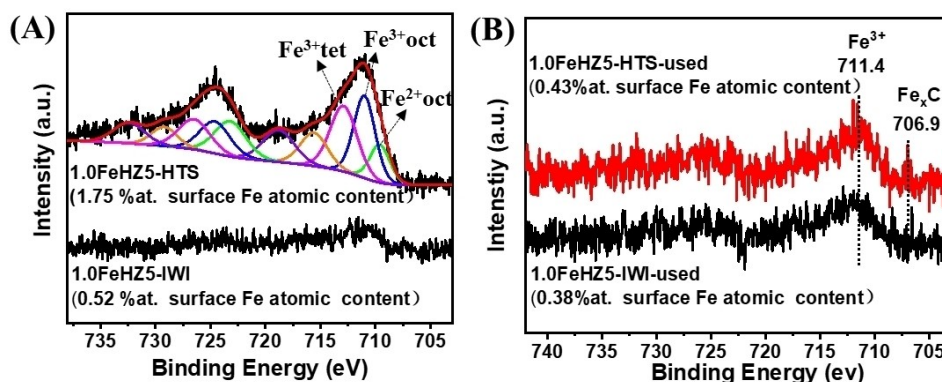


Figure 8. XPS spectra in the Fe 2p region of 1.0Fe/HZ5-IWI and 1.0Fe/HZ5-HTS catalysts before and after EDH reaction. (oct, octahedral; tet, tetrahedral).

1063 cm^{-1} is a little higher than that of Fe/HZ5-IWI, indicating that more isolated Fe sites are over Fe/HZ5-HTS. On the other hand, from the drift-CO characterization results in Figure S2, the bands at 1740–1750 cm^{-1} and 1940–1960 cm^{-1} appear over both Fe/HZ5-IWI and Fe/HZ5-HTS, which could be ascribed to the bridged CO on Fe atoms with the modes of $\text{Fe}_3(\text{CO})$ and $\text{Fe}_2(\text{CO})$,^[15a] respectively. And it could be found that the corresponding band intensity at 1738 cm^{-1} over Fe/HZ5-HTS is higher than that of Fe/HZ5-IWI, which indicates more isolated Fe^{3+} is over Fe/HZ5-HTS, in accordance with previous UV/Vis result.

The catalytic performance of various catalysts as a function of time on stream are shown in Figure 9. It is found that HZSM-5 is nearly inactive with merely 6.0% ethane conversion over EDH, which indicates the introduction of Fe active sites is essential. Besides, it is observed that the selectivity of ethylene over HZSM-5 is rather low with merely 43.3%, which may come from the strong Brønsted acid sites of HZSM-5, as characterized in Figure 3, resulting in overreaction of product ethylene to generate coke.

As for the Fe/HZ5 samples, it is observed that the ethylene selectivity all reaches to 75–90% and then keeps steady for about 1200 minutes regardless of Fe introduction way, while the corresponding C_2H_4 yield increases rapidly initially and reaches a maximum in about 30 minutes, then followed by a smooth decay to different extents. As for Fe/HZ5-IWI, the

ethylene yield is 8.2%, 20.3% and 29.2% at time 120 minutes for 0.5, 1.0 and 2.0Fe/HZ5-IWI, respectively (Table 3). And it is found that the corresponding specific reaction yield rate of ethylene normalized by Fe content over 0.5Fe/HZ5-IWI, 1.0Fe/HZ5-IWI and 2.0Fe/HZ5-IWI are 0.065 $\text{mmol C}_2\text{H}_4\text{s}^{-1}\text{g}_{\text{Fe}}^{-1}$, 0.078 $\text{mmol C}_2\text{H}_4\text{s}^{-1}\text{g}_{\text{Fe}}^{-1}$ and 0.054 $\text{mmol C}_2\text{H}_4\text{s}^{-1}\text{g}_{\text{Fe}}^{-1}$, respectively, which indicates that the ethylene generation rate and Fe content presents an obvious volcanic curve over Fe/HZ5-IWI. On the other hand, when Fe is introduced via hydrothermal post-treatment, the ethylene yield is 20.0%, 40.4% and 26.1% at time 120 minutes for 0.5, 1.0 and 2.0Fe/HZ5-HTS, and the corresponding specific reaction yield rate of ethylene normalized by Fe content presents in the order of 1.0Fe/HZ5-HTS (0.166 $\text{mmol C}_2\text{H}_4\text{s}^{-1}\text{g}_{\text{Fe}}^{-1}$) > 0.5Fe/HZ5-HTS (0.133 $\text{mmol C}_2\text{H}_4\text{s}^{-1}\text{g}_{\text{Fe}}^{-1}$) \gg 2.0Fe/HZ5-HTS (0.052 $\text{mmol C}_2\text{H}_4\text{s}^{-1}\text{g}_{\text{Fe}}^{-1}$), in which similar volcanic curve is observed between the ethylene generation rate and Fe content compared with that of Fe/HZ5-IWI. When Fe loading is high (2.0 wt%), the corresponding ethylene yield rate normalized by Fe content decreases obviously, which could be ascribed to formation of large inactive Fe_2O_3 particles, which is demonstrated by previous UV/Vis characterization result (Figure 7 and Table 2). In addition, it is found the corresponding specific reaction yield rate of ethylene normalized by Fe content over 1.0Fe/HZ5-HTS (0.166 $\text{mmol C}_2\text{H}_4\text{s}^{-1}\text{g}_{\text{Fe}}^{-1}$) is twice as much as 1.0Fe/HZ5-IWI (0.078 $\text{mmol C}_2\text{H}_4\text{s}^{-1}\text{g}_{\text{Fe}}^{-1}$), which demonstrates that the Fe/

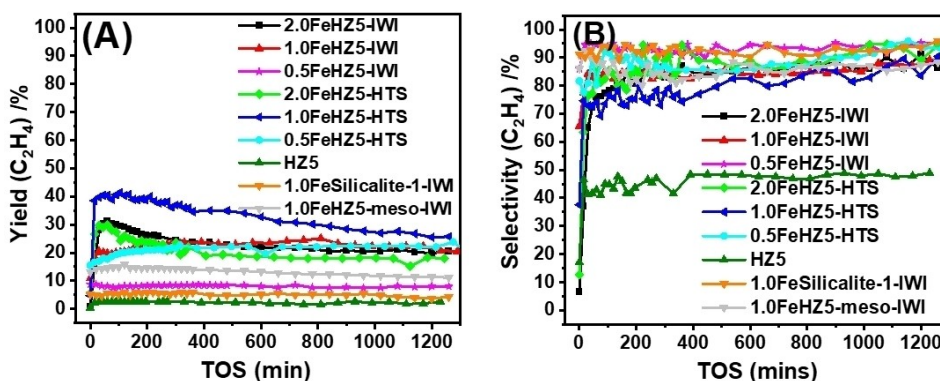


Figure 9. EDH performance of HZSM-5, Fe/HZ5-IWI and Fe/HZ5-HTS. Reaction conditions: 0.100 g catalyst and 0.500 g quartz sand (40–60 mesh), 10 mL/min 5% $\text{C}_2\text{H}_6/\text{Ar}$, 650 °C.

No.	Samples	Conv. (C_2H_6) ^[a] [%]	Yield (C_2H_4) ^[a] [%]	Sel. (C_2H_4) ^[a] [%]	Rate ^[b] [$\text{mmol C}_2\text{H}_4\text{s}^{-1}\text{g}_{\text{Fe}}^{-1}$]
1	HZSM-5	6.0	2.6	43.3	–
2	0.5Fe/HZ5-IWI	8.6	8.2	95.1	0.065
3	1.0Fe/HZ5-IWI	24.6	20.3	82.6	0.078
4	2.0Fe/HZ5-IWI	36.9	29.2	79.0	0.054
5	0.5Fe/HZ5-HTS	22.4	20.0	89.6	0.133
6	1.0Fe/HZ5-HTS	53.4	40.4	75.7	0.166
7	2.0Fe/HZ5-HTS	31.0	26.1	84.0	0.052
8	1.0Fe/HZ5-meso-HTS	31.1	23.4	75.2	0.088
9	1.0Fe/Silicalite-1-HTS	6.1	5.7	93.5	0.021

[a] C_2H_6 conversion, C_2H_6 yield, C_2H_4 selectivity, CH_4 selectivity were collected under the 650 °C reaction condition after 120 mins, [b] Reaction rate was calculated based on the yield of C_2H_4 under 650 °C reaction condition.

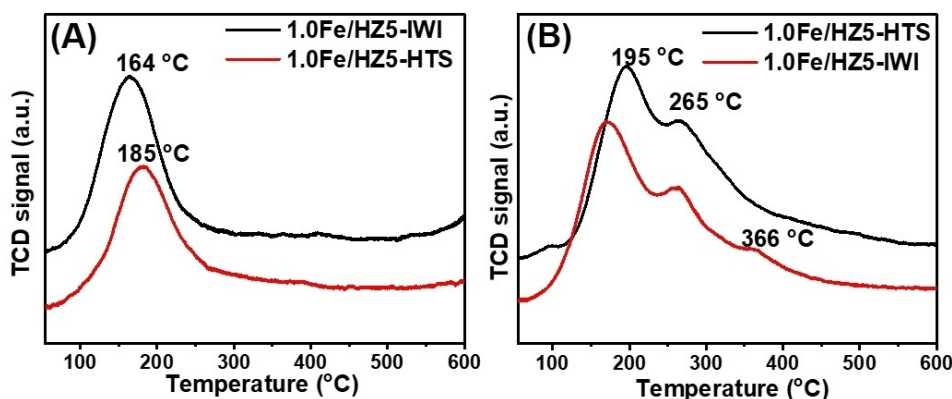


Figure 10. C_2H_6 -TPD (A) and C_2H_4 -TPD (B) profiles of 1.0Fe/HZ5-IWI and 1.0Fe/HZ5-HTS.

HZ5-HTS presents better catalytic performance compared with that of Fe/HZ5-IWI at the same Fe content, which could be ascribed to more isolated Fe^{3+} sites and exposing more Fe species in the surface over Fe/HZ5-HTS compared with Fe/HZ5-IWI (Figure 7 and Figure 8).

Besides, it is worth noting that the mesoporous volume over Fe/HZ5-HTS samples is obviously higher than that of Fe/HZ5-IWI samples based on BET characterization results (Table 1), which is mainly generated by alkaline dissolution of Si species in the hydrothermal treatment process. To further validate the influence of hierarchical pore, 1.0Fe/HZ5-meso-IWI with mesoporous is prepared (Table 1, No.8), it is found that the yield of ethylene is 23.4% and corresponding specific reaction yield rate of ethylene normalized by Fe content is $0.088 \text{ mmol } C_2H_4 s^{-1} g_{Fe}^{-1}$ (Table 3, No.8), which is a little higher than 1.0Fe/HZ5-IWI, but still much lower than 1.0Fe/HZ5-HTS, which indicates the promotion effect via improving diffusion confinement with hierarchical pore is limited, since the microporous structure of HZSM-5 ($0.51 \times 0.55 \text{ nm}$ and $0.53 \times 0.56 \text{ nm}$) is theoretically enough for ethane and ethylene diffusion.

In addition, 1.0Fe/Silicalite-1-IWI without introduction Al sites is also prepared as contrast. The yield of ethylene is only 5.7% and the corresponding specific reaction yield rate of ethylene normalized by Fe content is only $0.021 \text{ mmol } C_2H_4 s^{-1} g_{Fe}^{-1}$ (Table 3, No.9), which is much lower than that of Fe/HZ5, indicating the existence of Al to generate Brønsted acid sites is essential, since the implantation of Fe species is around the Si–O(H)–Al Brønsted acid sites. The merely Silicalite-1 as support would result in the aggregation of Fe species.

On the other hand, the catalytic performance including conversion and selectivity could be influenced by corresponding adsorption/desorption behavior of the ethane and ethylene on the surface. It is generally accepted that the adsorption of ethane would increase the residence time further facilitating the reaction, and coke deposition is formed by overreaction of the ethylene.^[10b] Correspondingly, C_2H_6 -TPD and C_2H_4 -TPD experiments over the 1.0Fe/HZ5-IWI and 1.0Fe/HZ5-HTS catalysts are investigated. As shown in Figure 10A, it could be found that the desorption temperature of ethane over 1.0Fe/HZ5-HTS (185°C) is a little higher than that of 1.0Fe/HZ5-IWI (164°C),

which would increase its residence time on the surface correspondingly thus resulting in the higher conversion. On the other hand, as for C_2H_4 -TPD (Figure 10B), two C_2H_4 desorption peaks around 195°C and 265°C are all observed over the 1.0Fe/HZ5-IWI and 1.0Fe/HZ5-HTS, while a higher C_2H_4 -TPD desorption peak at 366°C is observed over 1.0Fe/HZ5-IWI, which may further facilitate the overreaction of the ethylene to generate coke deposition in the presence of Brønsted acid sites.

The amount of deposited carbon on the 1.0Fe/HZ5-IWI and 1.0Fe/HZ5-HTS after 1260 mins time on stream is further investigated by TG, as shown in Figure 11. The TG loss weight curve could be divided into two parts, the physical adsorbed H_2O below 100°C and the coke deposition between 200 to 800°C . It could be found that the coke deposition (2.77%) and weight loss temperature peak (558°C) of 1.0Fe/HZ5-HTS is obviously lower than that of 1.0Fe/HZ5-IWI (4.42% and 664°C , respectively) after the same reaction time. The less coke deposition would facilitate the life stability of Fe/HZ5-HTS.

Figure 8B shows the Fe 2p XPS results of used samples, it could be found that the corresponding Fe 2p signal intensity is obviously lower than that of fresh samples, which may be ascribed to that the adsorption of organic substance or coke

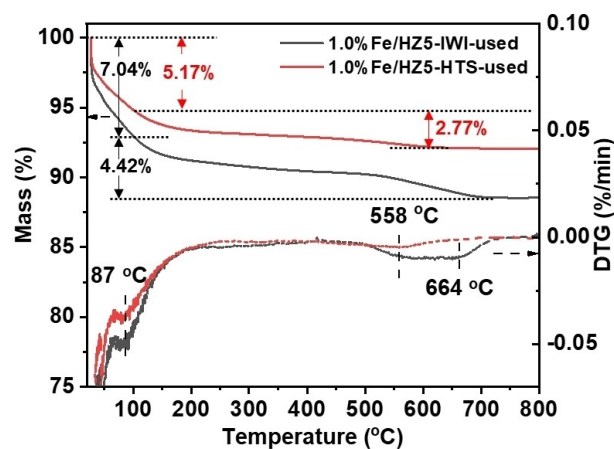


Figure 11. TG and DTG curves of Fe/HZ5-IWI and Fe/HZ5-HTS.

cover in the surface. Besides, both 1.0Fe/HZ5-HTS and 1.0Fe/HZ5-IWI catalysts show major peak at 711.4 eV corresponding to isolated Fe^{3+} , indicating that isolated Fe^{3+} species as main active sites keep stable after reaction. In addition, it is reported that carburized iron (Fe_xC) is suggested to be catalytically active sites on the dehydrogenation of ethane^[10a] and dehydroaromatization of CH_4 .^[16] And it could be found a minor peak appears at 706.9 eV over 1.0Fe/HZ5-HTS, which could be ascribed to Fe_xC species generated during EDH, and the corresponding Fe_xC species peak intensity is higher than that of 1.0Fe/HZ5-IWI, which could result in the better EDH catalytic performance of Fe/HZ5-HTS.

To further investigate the time-on-stream stability of Fe/HZ5-HTS, 0.5Fe/HZ5-HTS is evaluated, and corresponding catalytic result is shown in Figure 12. It is surprised to find that the catalytic performance of 0.5Fe/HZ5-HTS keeps stable and is not deactivated during 6000 minutes time-on-stream, which indicates Fe/HZ5-HTS is a high-performance catalyst.

Conclusion

In summary, a non-noble metal Fe supported HZSM-5 catalysts, via conventional incipient wetness impregnation and hydrothermal post-treatment method, are systematic investigated in the non-oxidative dehydrogenation of ethane to ethylene. In comparison with Fe/HZ5-IWI via incipient wetness impregnation, Fe/HZ5-HTS with low Fe content via hydrothermal post-treatment exhibits superior catalytic activity and a long catalyst stability with 6000 minutes time-on-stream. And 1.0Fe/HZ5-HTS shows the highest C_2H_4 yield with $0.166 \text{ mmol C}_2\text{H}_4 \text{ s}^{-1} \text{ g}_{\text{Fe}}^{-1}$ over various Fe loading, which is twice as much as that of 1.0Fe/HZ5-IWI with $0.078 \text{ mmol C}_2\text{H}_4 \text{ s}^{-1} \text{ g}_{\text{Fe}}^{-1}$. Based on the various characterizations methods including XPS, UV/Vis, H_2 -TPR, TEM, EDS and XPS characterizations, it is found that isolated Fe^{3+} species and carburized Fe species are active sites over EDH. And more disperse Fe species and exposing more Fe species in the

surface over Fe/HZ5-HTS are responsible for better EDH catalytic performance in comparison with Fe/HZ5-IWI. In addition, the lower ethylene desorption temperature and higher ethane desorption temperature over Fe/HZ5-HTS could suppress the overreaction of the ethylene to generate coke and increase corresponding residence reaction time, respectively.

Experimental Section

HZSM-5 (Si/Al=29) was purchased from FUYU (Zhangjiang) New Materials Technology Co., Ltd. Two sets of Fe/HZ5 catalysts were prepared via hydrothermal treatment process and conventional incipient wetness impregnation, respectively.

In the first catalyst set, the Fe/HZ5-HTS catalysts with different Fe loading (0.5, 1.0 and 2.0 wt%) were synthesized through hydrothermal post-treatment of the conventional sample HZSM-5 according to the literature.^[17] HZSM-5 was suspended in an aqueous solution that contained TPABr, ethylamine (EA) and $\text{Fe}(\text{NO}_3)_3 \cdot 9\text{H}_2\text{O}$ in a PTFE lining, the typical aqueous solution has the following molar composition: x Fe: 1.0 SiO_2 : 0.04 TPABr: 0.07 EA:10 H_2O , x=0.0054, 0.0107 and 0.0214. Then the mixture was stirred for half an hour. The PTFE lining was put into a stainless-steel autoclave and crystallized at 170°C for 24 h. Then the product was recovered by filtration, drying, and calcinations (550°C) for 6 h in air. The calcined sample was denoted as x Fe/HZ5-HTS (x represents the Fe weight loading with 0.5, 1.0 and 2.0 wt%).

In the second catalyst set, the Fe/HZ5-IWI catalysts with different Fe loadings (0.5, 1.0 and 2.0 wt%) were prepared by conventional incipient wetness impregnation method using aqueous solutions of $\text{Fe}(\text{NO}_3)_3 \cdot 9\text{H}_2\text{O}$. After impregnation, the catalysts were dried at 80°C in air overnight and further calcinations at 550°C for 6 h in air. The calcined sample was denoted as x Fe/HZ5-IWI (x represents the Fe weight loading with 0.5, 1.0 and 2.0 wt%).

As contrast, Fe/Silicalite-1-IWI with 1.0 wt% Fe loading was also prepared via incipient wetness impregnation procedure the same as Fe/HZ5-IWI without introduction Al species. In addition, hierarchical pore Fe/HZ5-meso with 1.0 wt% Fe loading was prepared as follows: firstly, HZSM-5-meso was prepared according to the procedure described in the above first catalyst preparation with TPABr, ethylamine, but without introducing the Fe precursor.^[17] Then the product was recovered by filtration, drying, and calcinations (550°C), finally to obtain the hierarchical pore HZSM-5-meso. Then 1.0 wt% Fe was supported over above HZSM-5-meso via incipient wetness impregnation method. Then sample was dried at 80°C in air overnight and further calcinations at 550°C for 6 h in air. Finally, the calcined sample was denoted 1.0Fe/HZ5-meso-IWI. Experimental Details.

The X-ray diffraction (XRD) patterns were measured on a Rigaku Ultima IV diffractometer using $\text{Cu K}\alpha$ radiation and a nickel filter in the 2θ angle range from 5° to 60° at 35 kV and 25 mA. Inductively coupled plasma (ICP) atomic emission spectroscopy was performed on a Thermo IRIS Intrepid II XSP atomic emission spectrometer. Nitrogen physisorption was carried out on a BEL-MAX instrument at 77 K after outgassing the samples for 6 h under vacuum at 300°C . The UV-Visible diffuse reflectance spectra (UV/Vis) were recorded on a Shimadzu UV-2400PC spectrophotometer using BaSO_4 plate as a reference. The temperature programmed experiments were tested on an AutoChem II 2920 instrument equipped with a thermal conductivity detector. For NH_3 -TPD, typically, 100 mg of sample was pre-treated in helium stream ($30 \text{ mL}\cdot\text{min}^{-1}$) at 550°C for 1 h. The adsorption of NH_3 was carried out at 50°C for 1 h, followed by purging with helium at 100°C for 2 h to remove

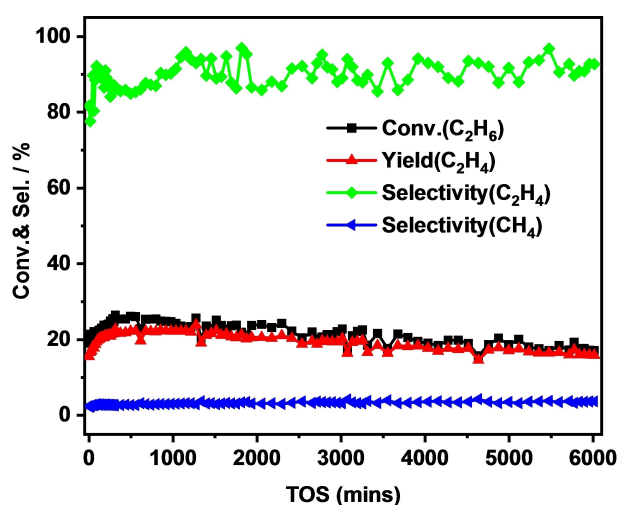


Figure 12. The catalytic stability evaluation of 0.5Fe/HZ5-HTS over ethane dehydrogenation to ethylene.

physisorbed NH_3 from the catalyst surface. The TPD profile was recorded at a heating rate of 5°C min^{-1} from 100 to 550°C . For the C_2H_6 -TPD and C_2H_4 -TPD, 100 mg of each sample was pretreated at 650°C for 1 h under 5% H_2/Ar and cooled to 50°C , then exposed to C_2H_6 or C_2H_4 flow for 30 min until saturation, followed by purging with He for 30 min to remove physisorbed C_2H_6 or C_2H_4 . The temperature was then ramped to 600°C at 10°C/min and held for 1 h until complete desorption of C_2H_6 or C_2H_4 . As for H_2 -TPR, typically, 100 mg of sample was pretreated in He at 300°C for 60 min followed by cooling down to 50°C , then sample was reduced in a flow of H_2/He mixture (5 vol.% H_2) from 50 to 850°C with a heating rate of 10°C/min . Transmission electron microscopy (TEM) images were recorded by a FEI Talos F200S G2 at an acceleration voltage of 200 kV, and energy-dispersive X-ray spectroscopy (EDS) elemental mappings were produced on a SuperX 2 SDD EDX detector. The surface compositions of the samples were measured by X-ray photoelectron spectroscopy (XPS) on a ESCALAB 250.

Catalytic performance evaluation was carried out at the atmospheric pressure in a quartz tubular fixed-bed reactor with 7 mm inner diameter and 63 cm length. A mixture of 100 mg catalysts and 500 mg quartz sand with 40–60 mesh size distribution was loaded in the reactor. The catalyst bed temperature was measured by a thermocouple centered axially inside the reactor. Before reaction, catalyst was pretreated with 30 mL/min 5% H_2 at 650°C for 2 h, then 10 mL/min 5% $\text{C}_2\text{H}_6/\text{Ar}$ was introduced. The reaction products were analyzed by an online GC-2014 equipped with an FID detector to detect hydrocarbons and a TCD detector to detect hydrogen. The carbon balance calculated from the ratio of sum of the reaction products to educts was over 95% for all catalysts tested during reaction process. The ethane conversion ($\text{Conv.}(\text{C}_2\text{H}_6)$), ethane selectivity ($\text{Sel.}(\text{C}_2\text{H}_4)$), ethane yield ($\text{Y.}(\text{C}_2\text{H}_4)$), methane selectivity ($\text{Sel.}(\text{CH}_4)$) were calculated according to Equations (1)–(4):

$$\text{Conv.}(\text{C}_2\text{H}_6) (\%) = ([\text{C}_2\text{H}_6]_{\text{in}} - [\text{C}_2\text{H}_6]_{\text{out}}) / [\text{C}_2\text{H}_6]_{\text{in}} \times 100 \quad (1)$$

$$\text{Sel.}(\text{C}_2\text{H}_4) (\%) = [\text{C}_2\text{H}_4] / ([\text{C}_2\text{H}_6]_{\text{in}} - [\text{C}_2\text{H}_6]_{\text{out}}) \times 100 \quad (2)$$

$$\text{Sel.}(\text{CH}_4) (\%) = (0.5 \times [\text{CH}_4]) / ([\text{C}_2\text{H}_6]_{\text{in}} - [\text{C}_2\text{H}_6]_{\text{out}}) \times 100 \quad (3)$$

$$\text{Yield}(\text{C}_2\text{H}_4) (\%) = [\text{C}_2\text{H}_4] / [\text{C}_2\text{H}_6]_{\text{in}} \times 100 \quad (4)$$

where $[\text{C}_2\text{H}_6]_{\text{in}}$ and $[\text{C}_2\text{H}_6]_{\text{out}}$ represent the ethane concentration in the inlet and outlet gas flow, $[\text{C}_2\text{H}_4]$, $[\text{CH}_4]$ are ethylene and methane concentration in the outlet gas flow, respectively.

Acknowledgements

We gratefully acknowledge the National Natural Science Foundation of China (U19B2003, 21902027 and 21902029), the Foundation of State Key Laboratory of High-Efficiency Utilization of Coal and Green Chemical Engineering (2019-KF-23), Natural Science Foundation of Fujian Province (2020 J01443 and 2020 J05121), Educational Committee of Fujian Province (JAT200042) and Fuzhou University Testing Fund of precious apparatus (2021T006).

Conflict of Interest

The authors declare no conflict of interest.

Keywords: Ethane dehydrogenation · Fe/ZSM-5 · hydrothermal post-treatment · highly dispersed Fe

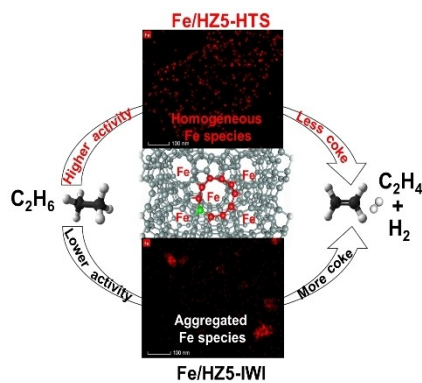
- [1] a) V. N. Cavaliere, M. G. Crestani, B. Pinter, M. Pink, C.-H. Chen, M.-H. Baik, D. J. Mindiola, *J. Am. Chem. Soc.* **2011**, *133*, 10700–10703; b) E. Gomez, B. Yan, S. Kattel, J. G. Chen, *Nat. Chem. Rev.* **2019**, *3*, 638–649.
- [2] a) M. M. Bhasin, J. H. McCain, B. V. Vora, T. Imai, P. R. Pujadó, *Appl. Catal. A* **2001**, *221*, 397–419; b) F. Cavani, N. Ballarini, A. Cericola, *Catal. Today* **2007**, *127*, 113–131.
- [3] a) Y. Dai, X. Gao, Q. Wang, X. Wan, C. Zhou, Y. Yang, *Chem. Soc. Rev.* **2021**, *50*, 5590–5630; b) H. Saito, Y. Sekine, *RSC Adv.* **2020**, *10*, 21427–21453; c) Y. Gao, X. Wang, J. Liu, C. Huang, K. Zhao, Z. Zhao, X. Wang, F. Li, *Sci. Adv.* **2020**, *6*; d) D. Melzer, P. Xu, D. Hartmann, Y. Zhu, N. D. Browning, M. Sanchez-Sanchez, J. A. Lercher, *Angew. Chem. Int. Ed.* **2016**, *55*, 8873–8877; *Angew. Chem.* **2016**, *128*, 9019–9023; e) D. Melzer, P. Xu, D. Hartmann, Y. Zhu, N. D. Browning, M. Sanchez-Sanchez, J. A. Lercher, *Angew. Chem. Int. Ed.* **2016**, *55*, 8873–8877; *Angew. Chem.* **2016**, *128*, 9019–9023; f) Y. Gao, X. Wang, J. Liu, C. Huang, K. Zhao, Z. Zhao, X. Wang, F. Li, *Sci. Adv.* **2020**, *6*, eaaz9339.
- [4] a) J. Lu, B. Fu, M. C. Kung, G. Xiao, J. W. Elam, H. H. Kung, P. C. Stair, *Science* **2012**, *335*, 1205; b) A. Siahvashi, D. Chesterfield, A. A. Adesina, *Ind. Eng. Chem. Res.* **2013**, *52*, 4017–4026; c) J. T. Grant, C. A. Carrero, F. Goetl, J. Venegas, P. Mueller, S. P. Burt, S. E. Specht, W. P. McDermott, A. Chierogato, I. Hermans, *Science* **2016**, *354*, 1570; d) Z. Li, A. F. W. Peters, A. E. Platero-Prats, J. Liu, C.-W. Kung, H. Noh, M. R. DeStefano, N. M. Schweitzer, K. W. Chapman, J. T. Hupp, O. K. Farha, *J. Am. Chem. Soc.* **2017**, *139*, 15251–15258; e) Y. Bian, M. Kim, T. Li, A. Asthagiri, J. F. Weaver, *J. Am. Chem. Soc.* **2018**, *140*, 2665–2672; f) S. Chen, L. Zeng, R. Mu, C. Xiong, Z.-J. Zhao, C. Zhao, C. Pei, L. Peng, J. Luo, L.-S. Fan, J. Gong, *J. Am. Chem. Soc.* **2019**, *141*, 18653–18657.
- [5] a) J. J. H. B. Sattler, J. Ruiz-Martinez, E. Santillan-Jimenez, B. M. Weckhuysen, *Chem. Rev.* **2014**, *114*, 10613–10653; b) M.-J. Cheng, W. A. Goddard, *J. Am. Chem. Soc.* **2015**, *137*, 13224–13227.
- [6] a) S. De Rossi, M. Pia Casaletto, G. Ferraris, A. Cimino, G. Minelli, *Appl. Catal. A* **1998**, *167*, 257–270; b) J. Gascón, C. Téllez, J. Herguido, M. Menéndez, *Appl. Catal. A* **2003**, *248*, 105–116; c) N. Mimura, M. Okamoto, H. Yamashita, S. T. Oyama, K. Murata, *J. Phys. Chem. B* **2006**, *110*, 21764–21770; d) L. Shi, G.-M. Deng, W.-C. Li, S. Miao, Q.-N. Wang, W.-P. Zhang, A.-H. Lu, *Angew. Chem. Int. Ed.* **2015**, *54*, 13994–13998; *Angew. Chem.* **2015**, *127*, 14200–14204; e) K. Searles, K. W. Chan, J. A. Mendes Burak, D. Zemlyanov, O. Safonova, C. Copéret, *J. Am. Chem. Soc.* **2018**, *140*, 11674–11679; f) N. M. Phadke, E. Mansoor, M. Bondil, M. Head-Gordon, A. T. Bell, *J. Am. Chem. Soc.* **2019**, *141*, 1614–1627; g) A. S. Al-Awadi, S. M. Al-Zahrani, A. M. El-Toni, A. E. Abasaheed, *Catalysts* **2020**, *10*; h) A. Al-Mamoori, S. Lawson, A. A. Rownaghi, F. Rezaei, *Appl. Catal. B: Environ.* **2020**, *278*, 119329; i) N. W. Felvey, M. J. Meloni, C. X. Kronawitter, R. C. Runnebaum, *Catal. Sci. Technol.* **2020**, *10*, 5069–5081; j) Y. He, Z. Yang, Z. Liu, P. Wang, M. Guo, J. Ran, *ChemistrySelect* **2020**, *5*, 2232–2239; k) Z. Maeno, S. Yasumura, X. Wu, M. Huang, C. Liu, T. Toyao, K.-i. Shimizu, *J. Am. Chem. Soc.* **2020**, *142*, 4820–4832; l) Y. Nakaya, J. Hirayama, S. Yamazoe, K.-i. Shimizu, S. Furukawa, *Nat. Commun.* **2020**, *11*, 2838; m) Z. Feng, X. Liu, Y. Wang, C. Meng, *Molecules* **2021**, *26*.
- [7] a) P. L. De Cola, R. Gläser, J. Weitkamp, *Appl. Catal. A* **2006**, *306*, 85–97; b) G. Siddiqi, P. Sun, V. Galvita, A. T. Bell, *J. Catal.* **2010**, *274*, 200–206; c) P. Sun, G. Siddiqi, M. Chi, A. T. Bell, *J. Catal.* **2010**, *274*, 192–199; d) X. Liu, W.-Z. Lang, L.-L. Long, C.-L. Hu, L.-F. Chu, Y.-J. Guo, *Chem. Eng. J.* **2014**, *247*, 183–192; e) J. J. H. B. Sattler, I. D. Gonzalez-Jimenez, L. Luo, B. A. Stears, A. Malek, D. G. Barton, B. A. Kilos, M. P. Kaminsky, T. W. G. M. Verhoeven, E. J. Koers, M. Baldus, B. M. Weckhuysen, *Angew. Chem. Int. Ed.* **2014**, *53*, 9251–9256; *Angew. Chem.* **2014**, *126*, 9405–9410; f) V. J. Cybulskis, B. C. Bukowski, H.-T. Tseng, J. R. Gallagher, Z. Wu, E. Wegener, A. J. Kropf, B. Ravel, F. H. Ribeiro, J. Greeley, J. T. Miller, *ACS Catal.* **2017**, *7*, 4173–4181; g) G. Sun, Z.-J. Zhao, R. Mu, S. Zha, L. Li, S. Chen, K. Zang, J. Luo, Z. Li, S. C. Purdy, A. J. Kropf, J. T. Miller, L. Zeng, J. Gong, *Nat. Commun.* **2018**, *9*, 4454.
- [8] a) C. T. W. Chu, C. D. Chang, *J. Phys. Chem.* **1985**, *89*, 1569–1571; b) H. Vankoningsveld, H. Vanbekkum, J. C. Jansen, *Acta Crystallogr. Sect. B* **1987**, *43*, 127–132; c) M. Bjørgen, S. Svelle, F. Joensen, J. Nerlov, S. Kolboe, F. Bonino, L. Palumbo, S. Bordiga, U. Olsbye, *J. Catal.* **2007**, *249*, 195–207.
- [9] a) J. Pérez-Ramírez, F. Kapteijn, A. Brückner, *J. Catal.* **2003**, *218*, 234–238; b) J. Pérez-Ramírez, E. V. Kondratenko, *Chem. Commun.* **2003**, 2152–2153; c) R. Bulánek, B. Wichterlová, K. Novoveská, V. Kreibich, *Appl. Catal.*

- A **2004**, 264, 13–22; d) P. Sazama, N. K. Sathu, E. Tabor, B. Wichterlová, Š. Sklenák, Z. Sobalík, *J. Catal.* **2013**, 299, 188–203.
- [10] a) L.-C. Wang, Y. Zhang, J. Xu, W. Diao, S. Karakalos, B. Liu, X. Song, W. Wu, T. He, D. Ding, *Appl. Catal. B* **2019**, 256, 117816; b) Z. Yang, H. Li, H. Zhou, L. Wang, L. Wang, Q. Zhu, J. Xiao, X. Meng, J. Chen, F.-S. Xiao, *J. Am. Chem. Soc.* **2020**, 142, 16429–16436.
- [11] S. Takenaka, M. Serizawa, K. Otsuka, *J. Catal.* **2004**, 222, 520–531.
- [12] a) J. G. Post, J. H. C. van Hooff, *Zeolites* **1984**, 4, 9–14; b) A. S. Al-Dughaiter, H. de Lasa, *Ind. Eng. Chem. Res.* **2014**, 53, 15303–15316.
- [13] a) H.-Y. Lin, Y.-W. Chen, C. Li, *Thermochim. Acta* **2003**, 400, 61–67; b) C. Messi, P. Carniti, A. Gervasini, *J. Therm. Anal. Calorim.* **2008**, 91, 93–100.
- [14] a) M. S. Kumar, M. Schwidder, W. Grünert, A. Brückner, *J. Catal.* **2004**, 227, 384–397; b) X. Shi, H. He, L. Xie, *Chin. J. Catal.* **2015**, 36, 649–656.
- [15] a) Y. Xu, X. Yuan, M. Chen, A. Dong, B. Liu, F. Jiang, S. Yang, X. Liu, *J. Catal.* **2021**, 396, 224–241; b) H. Xia, K. Sun, K. Sun, Z. Feng, W. X. Li, C. Li, *J. Phys. Chem. C* **2008**, 112, 9001–9005; c) K. Sun, H. Xia, Z. Feng, R. van Santen, E. Hensen, C. Li, *J. Catal.* **2008**, 254, 383–396.
- [16] P. Tan, *J. Catal.* **2016**, 338, 21–29.
- [17] L. Wu, X. Deng, S. Zhao, H. Yin, Z. Zhuo, X. Fang, Y. Liu, M. He, *Chem. Commun.* **2016**, 52, 8679–8682.

Manuscript received: May 24, 2021
Revised manuscript received: July 6, 2021
Accepted manuscript online: July 7, 2021
Version of record online: ■■■, ■■■■

FULL PAPERS

Hydrothermal post-treatment: A high-performance ethane non-oxidative dehydrogenation is prepared via hydrothermal post-treatment. Isolated Fe^{3+} species and carburized Fe species are active sites, and the excellent catalytic performance is ascribed to more disperse Fe species and exposing more Fe species in the surface.



Dr. L. Wu, Z. Fu, Z. Ren, J. Wei, Prof. X. Gao, Prof. L. Tan, Prof. Y. Tang*

1 – 11

Enhanced Catalytic Performance of Fe-containing HZSM-5 for Ethane Non-Oxidative Dehydrogenation via Hydrothermal Post-Treatment

